Experimental verification of leverage-type stiffness-controllable tuned mass damper using direct output feedback LQR control with time-delay compensation

Shih-Yu Chu[*], Shih-Wei Yeh[a], Lyan-Ywan Lu[b] and Chih-Hua Peng[c]

Department of Civil Engineering, National Cheng Kung University, No.1, University Road, Tainan, Taiwan

Abstract.   Vibration control using a tuned mass damper (TMD) is an effective technique that has been verified using analytical methods and experiments. It has been applied in mechanical, automotive, and structural applications. However, the damping of a TMD cannot be adjusted in real time. An excessive mass damper stroke may be introduced when the mass damper is subjected to a seismic excitation whose frequency content is within its operation range. The semi-active tuned mass damper (SATMD) has been proposed to solve this problem. The parameters of an SATMD can be adjusted in real time based on the measured structural responses and an appropriate control law. In this study, a stiffness-controllable TMD, called a leverage-type stiffness-controllable mass damper (LSCMD), is proposed and fabricated to verify its feasibility. The LSCMD contains a simple leverage mechanism and its stiffness can be altered by adjusting the pivot position. To determine the pivot position of the LSCMD in real time, a discrete-time direct output-feedback active control law that considers delay time is implemented. Moreover, an identification test for the transfer function of the pivot driving and control systems is proposed. The identification results demonstrate the target displacement can be achieved by the pivot displacement in 0-2 Hz range and the control delay time is about 0.1 s. A shaking-table test has been conducted to verify the theory and feasibility of the LSCMD. The comparisons of experimental and theoretical results of the LSCMD system show good consistency. It is shown that dynamic behavior of the LSCMD can be simulated correctly by the theoretical model and that the stiffness can be properly adjusted by the pivot position. Comparisons of experimental results of the LSCMD and passive TMD show the LSCMD with less demand on the mass damper stroke than that for the passive TMD.

Keywords: semi-active control; variable stiffness; mass damper; discrete-time optimal linear-quadratic regulator (LQR) control; direct output-feedback, time-delay compensation, leverage theorem; position control; servo motor

1. Introduction

Vibration control using a tuned mass damper (TMD), which is an effective technique that has been verified by numerous analytical methods and experiments, has been applied to mechanical, automotive, and structural applications (Chung *et al.* 2013a, Li *et al.* 2012, Moghaddas *et al.* 2011, Wang *et al.* 2003). In civil engineering, a TMD is mounted on the top floor of high-rise buildings to mitigate the amplitude of vibrations caused by seismic excitations for preventing discomfort or structural failure (Rakicevic *et al.* 2012, Marano and Greco 2011). The frequency of a TMD, which commonly includes a mass, a spring, and a damper, is tuned to that of the controlled building. When the building is excited by seismic excitations, the seismic energy is transmitted to the TMD and dissipated by the damper. Therefore, the damping of the TMD is crucial for reducing a large mass damper stroke. However, the damping of a TMD cannot be adjusted in real time. An excessive mass damper stroke may be introduced when the mass damper is subjected to seismic excitation whose frequency content is within its operation range. To avoid this problem, the hybrid mass damper (HMD) has been proposed.

The HMD is an active device consisting of an actuator and a TMD (Soleymani and Khodadadi 2014, Korkmaz 2011, Chu *et al.* 2002, 2005). The active force applied to the TMD's mass in real time is computed based on the measured structural responses and an appropriate control law. As a result, the mass damper stroke can be adaptively controlled by the active force. HMDs generally outperform TMDs. However, active devices usually need a large driving force and a lot of control energy. To create TMDs that can be altered in real time and have low control energy, some researchers have proposed the semi-active tune mass damper (SATMD).

SATMDs are TMDs integrated with a semi-active (or smart) device. The semi-active device is used to adjust the parameters of a TMD, such as damping or stiffness, in real time. SATMDs thus usually provide an adjustable passive

---

[*]Corresponding author, Associate Professor
  E-mail: sychu@mail.ncku.edu.tw
[a]Ph.D. Candidate
  E-mail: n68981042@mail.ncku.edu.tw
[b]Professor
  E-mail: lylu@mail.ncku.edu.tw
[c]Master of Science
  E-mail: burst1986@gmail.com

force during seismic excitations. The SATMD is different from the HMD in that the adjustable passive force is produced by regulating the parameters of a TMD with a control law. The control energy required for the SATMD is thus generally smaller than that of a HMD and SATMDs usually outperform TMDs.

Depending on the adjustable passive parameters of semi-active devices, the majority of the state-of-art SATMDs can be classified into two types: damping- and stiffness-controllable TMDs. For damping-controllable TMDs, the damper of a TMD is replaced by a magneto-rheological (MR) damper, whose damping force is adjusted by controlling the damper's inner magnet field (Ito *et al.* 2015, Lin *et al.* 2013, Kang *et al.* 2011). The damping of a harvester damper, an electromagnetic device that transforms mechanical vibration into electrical energy, is adjusted by altering inner resistance (Gonzalez-Buelga *et al.* 2014, Liu *et al.* 2013). The friction force of a variable-friction damper is adjusted by altering the clamping force of a passive friction damper (Lin *et al.* 2010, 2012). Damping-controllable TMDs are often used to reduce the excessive mass damper stroke. Chung *et al.* (2013b) implemented a variable-friction device to control the phase of a TMD for minimizing the off-tuned problem.

Several semi-active devices have been used in stiffness-controllable TMDs. The stiffness of a semi-active variable-stiffness device is adjusted by altering the angle of the springs, which are arranged in a rhombus shape (Deshmukh and Chandiramani 2014, Majcher 2014, Nagarajaiah and Sonmez 2007, Nagarajaiah and Varadarajan 2005). The frequency of an adaptive-length pendulum smart-tuned mass damper is adjusted by changing the current in a shape-memory alloy (SMA) wire or the effective length of the SMA wire (Pasala and Nagarajaiah 2014). The concept of a stiffness-controllable TMD is to adjust the stiffness (the tuned frequency) of the TMD to achieve better control performance. Moreover, the stiffness of a resettable variable-stiffness damper (RVSD) is switched on and then off at a large stroke (Lin *et al.* 2015, Chey *et al.* 2010). By resetting the stiffness of the TMD, the stored seismic energy can be dissipated.

The damping or stiffness of SATMDs is adjusted to achieve better control performance. In addition, the feasibility of some SATMDs introduced above are experimentally verified because the SATMDs consist of a control system with a control law and are more complex than passive devices. Chu *et al.* (2017) proposes a stiffness-controllable TMD called the leverage-type stiffness-controllable mass damper (LSCMD). The stiffness of the LSCMD is made adjustable by implementing a leverage mechanism with a movable pivot. The previous study demonstrated the LSCMD, HMD, and passive TMD were equally effective in reducing the story drift of the controlled structure; however, the LSCMD required less demand on the damper stroke than the passive TMD did. The LSCMD shows better control performance in numerical simulation. To experimentally verify the theoretical model and control performance of the LSCMD, the objective of this paper is to conduct a shaking-table test for the proposed LSCMD.

The rest of this paper is organized as follows. The concept and modeling of the LSCMD are introduced in Section 2. The equation of motion of the LSCMD and a numerical analysis method for the LSCMD system are given in Section 3. Section 4 describes the control law for the LSCMD. Sections 5 and 6 describe the prototype LSCMD and shaking-table test, respectively. The test results and control performance verification of the prototype LSCMD are discussed in Section 7. The conclusions are given in Section 8.

2. Leverage-type stiffness-controllable mass damper

2.1 Concept of LSCMD

In this section, the basic concept of the LSCMD is introduced. Fig. 1 depicts the leverage mechanism of the LSCMD, which includes a lever arm (member AC) and a moveable pivot (point P). Points A and C (the ends of the lever arm) are connected to a spring with a constant stiffness k_{d0} attached to a building and a mass damper, respectively. The fixed coordinate system in Fig. 1 has its origin in the middle of the lever arm. In Fig. 1, $x_{ds}(t)$ represents the mass damper stroke of the LSCMD; $x_{d0}(t)$ is the deformation of the spring; L is the original length of the lever arm; $x_p(t)$ is the displacement of pivot point P; $F_p(t)$ is a force required for driving the pivot. The length of the lever arm must be adjustable (e.g., telescopic) to fulfill the following conditions: (1) points A and C are constrained to move parallel to the Y-axis; (2) point P is constrained to move in the X direction. With this configuration, the equivalent stiffness of the LSCMD at point C is greater than the constant stiffness k_{d0} when the displacement of pivot point P is in the positive direction ($x_p(t)>0$); it is less when the displacement of pivot point P is in the negative direction ($x_p(t)<0$). Therefore, the equivalent stiffness $k_d(t)$ of the LSCMD can be adjusted by varying the displacement of pivot point P. A stiffness-controllable TMD is thus realized.
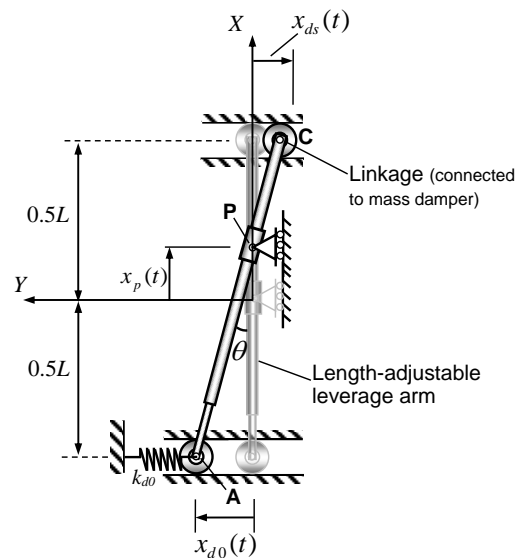

Fig. 1 Leverage mechanism

2.2 Modeling of LSCMD system

The governing equation of the LSCMD is derived in this section. Fig. 2 illustrates the mathematical model of the LSCMD system, where m_d and c_d denote the mass and damping coefficient of the LSCMD, respectively; $x_s(t)$ denotes the story drift of the structure; k_s and c_s denote the stiffness and damping coefficients of the structure, respectively; $\ddot{x}_g(t)$ denotes the ground acceleration. Note that the equivalent stiffness $k_d(t)$ of the LSCMD is further divided into two parts

$$k_d(t) = k_{d0} + \Delta k_d(x_p(t)) \tag{1}$$

where $\Delta k_d(x_p(t))$ represents a variable stiffness increment, which is related with the pivot displacement $x_p(t)$. In the physical world, the equivalent stiffness $k_d(t)$ must be positive, but the variable stiffness increment $\Delta k_d(x_p(t))$ can be either positive or negative. Thus, the controllability of the equivalent stiffness $k_d(t)$ of the LSCMD can be achieved. As shown in Figs. 1 and 2, the dynamic behavior of the LSCMD system can be described by a total of 4-degree-of-freedom (DOF), containing $x_s(t)$, $x_{ds}(t)$, $x_{d0}(t)$, and $x_p(t)$. The geometric relationship shown in Fig. 1 between $x_{ds}(t)$ and $x_{d0}(t)$ can be given as

$$x_{d0}(t) = \left(\frac{0.5L + x_p(t)}{0.5L - x_p(t)}\right)x_{ds}(t) \tag{2}$$

Consequently, the 4-DOF of the LSCMD system are reduced to three ($x_s(t)$, $x_{ds}(t)$, and $x_p(t)$). Next, after knowing the total number of DOFs, the governing equation of the LSCMD system can be derived by using Lagrange's equation of motion which can be expressed as

$$\frac{d}{dt}\left(\frac{\partial \pounds}{\partial \dot{q}_k}\right) - \frac{\partial \pounds}{\partial q_k} = Q_k \quad (k=1, 2, 3) \tag{3}$$

where $\pounds = (T\text{-}V)$ represents Lagrangian with T and V represents the total kinetic energy and potential energy of the system, respectively, i.e.

Leverage-type
stiffness-controllable device
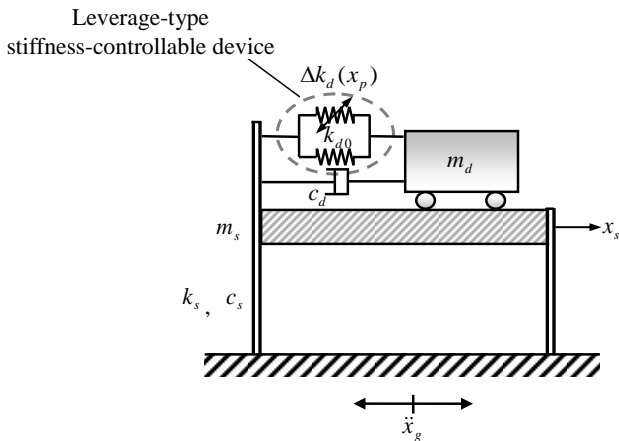
Fig. 2 Mathematical model of LSCMD system

$$T = \frac{1}{2}m_s(\dot{x}_s + \dot{x}_g)^2 + \frac{1}{2}m_d(\dot{x}_{ds} + \dot{x}_s + \dot{x}_g)^2 \tag{4}$$

$$\begin{aligned} V &= \frac{1}{2}x_{d0}^2 k_{d0} + \frac{1}{2}x_s^2 k_s \\ &= \frac{1}{2}\left(\frac{0.5L + x_p}{0.5L - x_p}\right)^2 x_{ds}^2 k_{d0} + \frac{1}{2}x_s^2 k_s \end{aligned} \tag{5}$$

Also, in Eq. (3), q_k represents the kth DOF in a generalized coordinate system, and Q_k represents corresponding non-conservative force for the kth DOF. If $q_1 = x_{ds}$, $q_2 = x_s$ and $q_3 = x_p$ are assigned, we have

$$Q_1 = -c_d\dot{x}_{ds}, \quad Q_2 = -c_s\dot{x}_s, \quad Q_3 = F_p \tag{6}$$

Substituting Eqs. (4)-(6) in Eq. (3), it shall lead to the following governing equations for the LSCMD system

$$\mathbf{M}\ddot{\mathbf{x}}(t) + \mathbf{C}\dot{\mathbf{x}}(t) + \mathbf{K}\mathbf{x}(t) + \mathbf{s}u_c(t) = -\mathbf{M}\mathbf{r}\,\ddot{x}_g(t) \tag{7}$$

$$F_p(t) = \left[\frac{0.5L^2 + Lx_p(t)}{(0.5L - x_p(t))^3}\right]k_{d0}\,x_{ds}(t)^2 \tag{8}$$

where

$$\mathbf{M} = \begin{bmatrix} m_s & 0 \\ m_d & m_d \end{bmatrix}, \quad \mathbf{C} = \begin{bmatrix} c_s & -c_d \\ 0 & c_d \end{bmatrix}, \quad \mathbf{K} = \begin{bmatrix} k_s & -k_{d0} \\ 0 & k_{d0} \end{bmatrix} \tag{9}$$

$$\mathbf{x}(t) = \begin{Bmatrix} x_s(t) \\ x_{ds}(t) \end{Bmatrix}, \quad \mathbf{s} = \begin{Bmatrix} -1 \\ 1 \end{Bmatrix}, \quad \mathbf{r} = \begin{Bmatrix} 1 \\ 1 \end{Bmatrix} \tag{10}$$

In Eq. (7), $\mathbf{M}$, $\mathbf{C}$, and $\mathbf{K}$ represent the mass, damping, and stiffness matrices of the LSCMD system, respectively; $u_c(t)$ represents the semi-active control force; $\mathbf{s}$ and $\mathbf{r}$ represent the semi-active control force and seismic force placement vectors, respectively. Note that in vector $\mathbf{x}(t)$, $x_s(t)$ represents the story drift of the structure, and $x_{ds}(t)$ represents the mass damper stroke of the LSCMD instead of relative-to-ground displacement. $F_p(t)$ represents the driving force of the pivot. As shown in Eq. (1), the equivalent stiffness $k_d(t)$ of the LSCMD is divided into two parts. Therefore, the matrix $\mathbf{K}$ contains the constant stiffness k_{d0} and the variable stiffness increment $\Delta k_d(x_p(t))$ is treated as the source of the semi-active control force. The semi-active control force $u_c(t)$ shown in Eq. (7) can be expressed as

$$u_c(t) = \Delta k_d(x_p(t))x_{ds}(t) \tag{11}$$

The relation between the variable stiffness increment $\Delta k_d(x_p(t))$ and the pivot displacement $x_p(t)$ can be described as (Lu *et al.* 2012)

$$\Delta k_d(t) = \left[\frac{2Lx_p(t)}{(0.5L - x_p(t))^2}\right]k_{d0}\ \text{for} -L/2 \leq x_p(t) \leq L/2 \tag{12}$$

3. Numerical analysis method for LSCMD system

In this section, a numerical analysis method that considers control delay time is introduced. First, Eq. (7) can be rewritten as a continuous-time state-space equation

$$\dot{\mathbf{z}}(t) = \mathbf{A}_c\mathbf{z}(t) + \mathbf{E}_c\ddot{x}_g(t) + \mathbf{S}_cu_c(t - t_d) \quad (13)$$

where

$$\mathbf{z}(t) = \begin{bmatrix} \mathbf{x}(t) \\ \dot{\mathbf{x}}(t) \end{bmatrix}, \quad \mathbf{A}_c = \begin{bmatrix} \mathbf{0} & \mathbf{I} \\ -\mathbf{M}^{-1}\mathbf{K} & -\mathbf{M}^{-1}\mathbf{C} \end{bmatrix},$$
$$\mathbf{E}_c = \begin{bmatrix} \mathbf{0} \\ -\mathbf{r} \end{bmatrix}, \quad \mathbf{S}_c = \begin{bmatrix} \mathbf{0} \\ \mathbf{M}^{-1}\mathbf{s} \end{bmatrix} \quad (14)$$

$\mathbf{z}(t)$ is a 4×1 state vector; $\mathbf{A}_c$ is a 4×4 continuous-time system state matrix; $\mathbf{E}_c$ is a 4×1 continuous-time seismic force placement matrix; $\mathbf{S}_c$ is a 4×1 continuous-time semi-active control force placement matrix. Note that $u_c(t-t_d)$ represents a delayed semi-active control force and t_d represents the delay time of the semi-active control force. In order to simulate responses of the LSCMD system in discrete time, the continuous-time state-space equation shown in Eq. (13) must be transformed into a discrete-time equation. Chu *et al.* (2005) proposed a discrete-time state-space equation that considers control delay time. According to the study, the discrete delay time t_d and the discrete-time state-space equation of the LSCMD system can be respectively written as

$$t_d = (\ell - m)\Delta t \quad (15)$$

$$\mathbf{z}[k+1] = \mathbf{A}_d\mathbf{z}[k] + \mathbf{E}_d\ddot{x}_g[k] + \mathbf{S}_{d1}u_c[k-\ell] + \mathbf{S}_{d2}u_c[k-\ell+1] \,(16)$$

where

$$\mathbf{A}_d = e^{\mathbf{A}_c\Delta t}, \quad \mathbf{E}_d = \mathbf{A}_c^{-1}[\mathbf{A}_d - \mathbf{I}]\mathbf{E}_c \quad (17)$$

$$\mathbf{S}_{d1} = \mathbf{A}_c^{-1}[\mathbf{A}_d - \mathbf{A}_d^m]\mathbf{S}_c, \quad \mathbf{S}_{d2} = \mathbf{A}_c^{-1}[\mathbf{A}_d^m - \mathbf{I}]\mathbf{S}_c \quad (18)$$

In the above equations, Δt is the sampling time of the system; ℓ ($\ell \geq 1$, $\ell \in \mathbb{N}$) is an integer that denotes the integer part of the delay time; m ($0 \leq m \leq 1$, $m \in \mathbb{R}$) is a real number that denotes the decimal part of the delay time; k is the time step; $\mathbf{A}_d$ represents the discrete-time system state matrix; $\mathbf{E}_d$ represents the discrete-time seismic force placement matrix; $\mathbf{S}_{d1}$ and $\mathbf{S}_{d2}$ represent the discrete-time control force placement matrices, which are related with the power of $\mathbf{A}_d$ to the order of the real number m.

4. Control Law for LSCMD

Eqs. (11) and (12) show that the semi-active control force $u_c(t)$ is related to the pivot displacement $x_p(t)$. The determination of the pivot displacement $x_p(t)$ is explained in this section. Chu *et al.* (2002, 2008) proposed a semi-active control law based on the discrete-time direct output-feedback optimal control algorithm with delayed control force. Similar to LQR control, the proposed feedback gain

matrix is determined by using an iterative method to solve simultaneously Lyapunov equations that consider the control delay time. Then, the semi-active control law is used to determine an active force $\bar{u}[k]$

$$\bar{u}[k] = \mathbf{GDz}[k] \quad (19)$$

where $\mathbf{G}$ represents a feedback gain matrix computed based on the proposed active control law and $\mathbf{D}$ represents a sensor placement matrix. Then, the active force $\bar{u}[k]$ shown in Eq. (19) is treated as the target control force for the LSCMD and assumed to be equal to the semi-active control force $u_c[k]$. The target stiffness increment $\Delta\bar{k}_d[k]$ is determined as the active force $\bar{u}[k]$ divided by the mass damper stroke x_{ds}

$$\Delta\bar{k}_d[k] = -\frac{\bar{u}[k]}{x_{ds}[k-1]}$$
$$= -\frac{\mathbf{GDz}[k]}{x_{ds}[k-1]} \quad (20)$$

Note that $x_{ds}[k-1]$ (delay of one step) is the mass damper stroke at the k-1 time step. The delay time of sensors is thus considered. Moreover, Eq. (12) can be rewritten as

$$\bar{x}_p[k] = \frac{L(\Delta\bar{k}_d[k] + k_{d0}) - \sqrt{4L^2\Delta\bar{k}_d[k]k_{d0}}}{2(\Delta\bar{k}_d[k] - k_{d0})} \quad (21)$$

The target pivot displacement $\bar{x}_p(t)$ can be solved using Eqs. (20) and (21). However, the target pivot displacement $\bar{x}_p[k]$ shown in Eq. (21) is an ideal value. The pivot displacement $x_p[k]$ may not be able to achieve the target pivot displacement $\bar{x}_p[k]$ in practice. The pivot displacement $x_p[k]$ should to be limited as

$$x_p[k] = \begin{cases} x_{p,\max} & \bar{x}_p[k] \geq x_{p,\max} \\ \bar{x}_p[k] & x_{p,\min} < \bar{x}_p[k] < x_{p,\max} \\ x_{p,\min} & \bar{x}_p[k] \leq x_{p,\min} \end{cases} \quad (22)$$
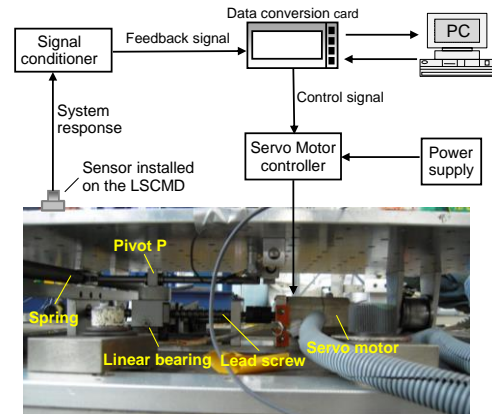

Fig. 3 Driving and control systems of prototype LSCMD

where $x_{p,\max}$ and $x_{p,\min}$ represent the upper and lower bounds of the pivot displacement, respectively. The pivot displacement $x_p[k]$ of the LSCMD can be determined by using Eqs. (20)-(22).

5. Prototype LSCMD

5.1 Prototype LSCMD

Fig. 3 depicts the leverage mechanism of the prototype LSCMD and its driving and control systems. The driving system drives the pivot to a target position. The components of the system are: a servo motor, a lead screw, and a linear bearing. The servo motor provides a torsional force to the lead screw, which drives the pivot to a target position. The linear bearing constrains the movement direction of the pivot. The control system sends pivot displacement commands to the driving system. The components of the control system are: a computer, a data conversion card, and a servo motor controller. The data conversion card (installed in the computer) converts analog signals to digital signals or vice versa. The computer computes the pivot displacement command based on the converted measured structural responses and the proposed control law and sends it to the servo motor controller through the conversion card.

Fig. 4 shows the motor controller of the prototype LSCMD. As shown, the servo motor controller consists of a programmable logic controller (PLC), a servo motor driver, and a power supply. The PLC is to transform the received control signal which is an analog voltage between +10V and -10V into a pulse command. Then, the pulse command is sent to the servo driver to generate a pulse signal which is used to drive the servo motor.

5.2 Identification of driving and control systems

As described above, the pivot displacement of the prototype LSCMD is to determine the stiffness increment Δk_d. Therefore, the performance of the driving and control systems is very important for the prototype LSCMD. A transfer function (or called frequency response function) which describes the relation between input and output signals can be utilized. To identify the transfer function
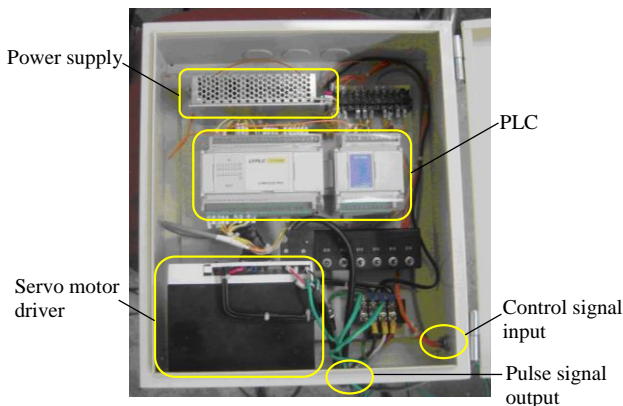
of the driving and control systems, the white-noise signal is adopted to the systems as control command $x_{p,r}$ while the pivot displacement $x_{p,m}$ is measured. The time histories of the control command $x_{p,r}$ and measured pivot displacement $x_{p,m}$ of a test are shown in Fig. 5, respectively. The bandwidth of the white noise shown in Fig. 5(a) is 0-50 Hz. By taking Fourier transforms of $x_{p,r}$ and $x_{p,m}$, the transfer function $H(\omega)$ of the system can be computed by

$$H(\omega) = \frac{U(x_{p,m})}{U(x_{p,r})} \qquad (23)$$

where, $H(\omega)$ is complex number and the phase angle ϕ_H can be determined by

$$\phi_H = \tan^{-1} \frac{\mathrm{Im}(H(\omega))}{\mathrm{Re}(H(\omega))} \qquad (24)$$

where, $\mathrm{Re}(H(\omega))$ and $\mathrm{Im}(H(\omega))$ represents the real part and image part of $H(\omega)$, respectively. Fig. 6 illustrates the corresponding identified results. Subplots (a) and (b) is the normalized amplitude and phase angle of the identified transfer function. In ideal condition, the normalized amplitude is 1 and the phase angle is zero. This means the control system can exactly achieve the control command. As shown in Fig. 6(a), the driving system can function normally in 0-1 Hz and Fig. 6(b) shows the delay time of the driving system is about 0.1 s.
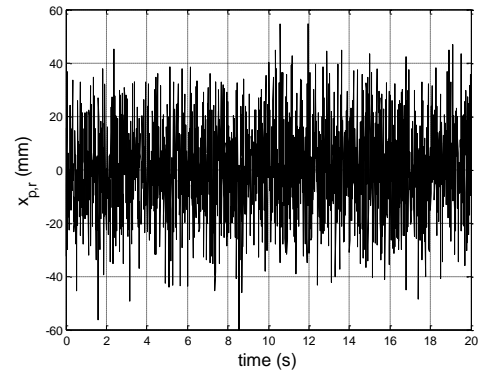
(a) Input command
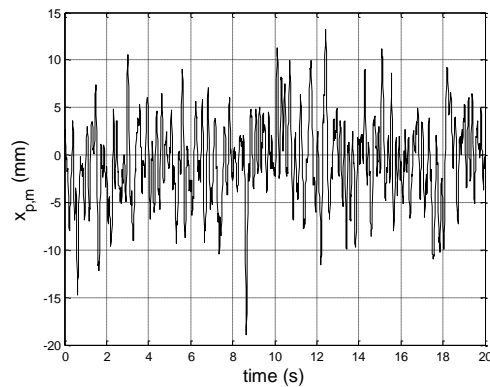
(b) Measured pivot displacement

Fig. 5 Time histories of input and output signals of driving and control systems
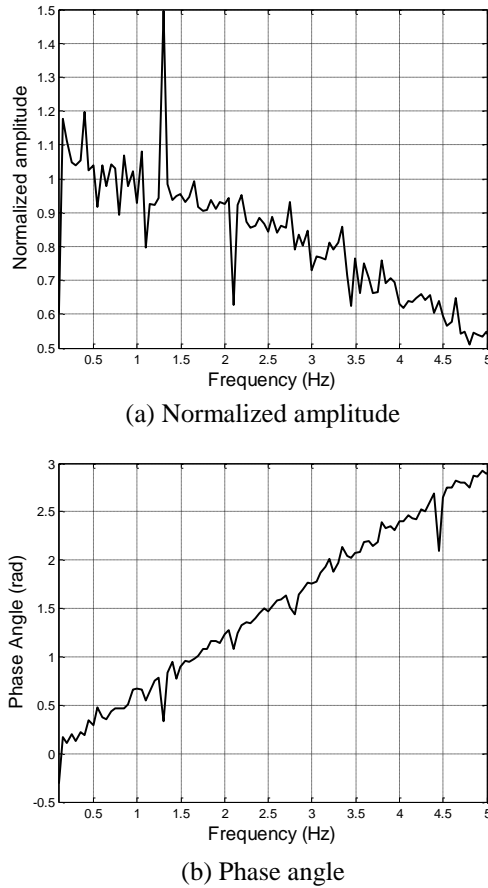

Fig. 4 Servo motor controller of prototype LSCMD

(a) Normalized amplitude

(b) Phase angle

Fig. 6 Identification transfer function results of Fig. 5

6. Shaking-table test for prototype LSCMD

To experimentally verify the derived discrete-time state-space equation in Section 3 and the feasibility of the LSCMD, a shaking-table test was thus conducted for a prototype LSCMD fabricated based on the concept given in Section 2. The shaking-table test setup, the design of feedback, and the selection of ground excitations are described in this section.

6.1 Test setup

Fig. 7 shows a photograph of the shaking-table test system for the LSCMD system. The LSCMD system consists of the prototype LSCMD and a rolling structure. The rolling structure includes a mass block, four rolling wheels, and four curved rail bearings. Table 1 lists the identified system parameters of the rolling structure, passive TMD and the prototype LSCMD, respectively, which were obtained from system identification tests before the shaking-table test. These parameters were also used for calculating the optimal control gain described in Section 4 and the numerical simulations. As shown in Table 1, the natural frequency of the rolling structure is identified to be 0.37 Hz, which is common for a high-rise structure. Note that the friction effect of the rolling structure is considered as an equivalent viscous damping ratio of 2%. To determine the frequency ratio and damping ratio for the passive part of

the prototype LSCMD, the optimization formulas proposed by Warburton (1982) are utilized

$$\gamma_{opt} = \frac{\sqrt{(1-0.5\mu_D)}}{1+\mu_D}, \quad \zeta_{d,opt} = \sqrt{\frac{\mu_d(1-0.25\mu_d)}{4(1+\mu_d)(1-0.5\mu_d)}} \quad (25)$$

Using Eq. (25), the optimal frequency ratio γ_{opt} and the damping ratio $\zeta_{d,opt}$ with a mass ratio of 0.1 are 0.89 and 15%, respectively. The identified frequency ratio of the LSCMD shown in Table 1 is 0.87. The friction effect of the prototype LSCMD system is also identified as an equivalent viscous damping ratio of 17%. Both values (0.87 and 17%) are close to the optimal parameters. Therefore, the unactivated LSCMD (i.e., $x_p(t)$=0) is approximately an optimal passive TMD system. The combined modal frequencies and modal damping ratios of the unactivated LSCMD are also tabulated in Table 1. Moreover, for practical concerns, the range of pivot displacement is restrained by the upper bound $x_{p,max}$ and lower bound $x_{p,min}$ to prevent the instability caused by the driving system.

The instrumentation of the prototype LSCMD for the shaking-table test is also shown in Fig. 7. Velocity sensors and accelerometers were installed on the rolling structure

Table 1 Parametric values of LSCMD system

|	Parameter	Value
Rolling structure	Mass, m_s (kg)	580
	Damping coefficient, c_s (N.s/m)	53.93
	Stiffness, k_s (N/m)	3134.70
	Damping ratio, ζ_s (%)	2
	Natural frequency, ω_s (Hz)	0.37
Passive TMD (unactivated LSCMD)	Mass ratio, $\mu_d = m_d/m_s$	0.1
	Damping ratio, ζ_d (%)	17
	Spring stiffness, k_{d0} (N/m)	236.17
	Frequency ratio, $\gamma = \omega_d/\omega_s$	0.87
	Modal frequencies $\begin{bmatrix} \omega_1 \\ \omega_2 \end{bmatrix}$ (Hz)	$\begin{bmatrix} 0.3 \\ 0.4 \end{bmatrix}$
	Modal damping ratios $\begin{bmatrix} \zeta_1 \\ \zeta_2 \end{bmatrix}$ (%)	$\begin{bmatrix} 9 \\ 9 \end{bmatrix}$
LSCMD	Length of lever arm, L (m)	0.274
	Range of frequency ratio, $(\gamma_{min}, \gamma_{max})$	(0.71, 1.06)
	Range of controllable stiffness, $(k_{d,min}, k_{d,max})$	$(0.67k_{d0}, 1.4965k_{d0})$
	Range of pivot displacement, $(x_{p,min}, x_{p,max})$ (m)	(-0.0137, 0.0138)
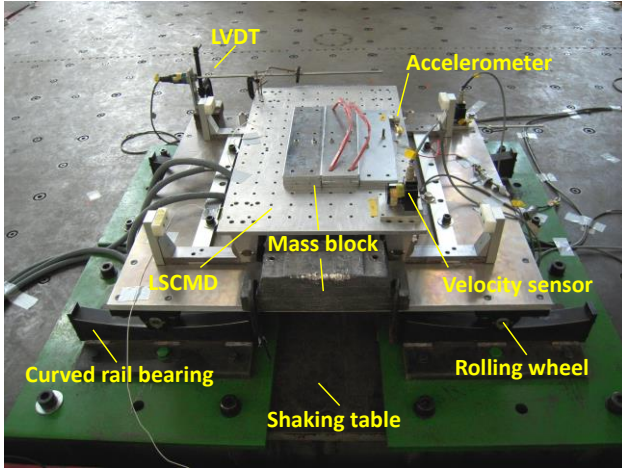
Fig. 7 Setup of shaking-table test for LSCMD system

and the prototype LSCMD. Moreover, an accelerometer was installed on the shaking table to measure the ground acceleration. Linear variable differential transformers (LVDTs) were installed to measure the pivot displacement x_p, the LSCMD stroke x_{ds}, and the story drift x_s of the rolling structure.

6.2 Design of feedback gains

The control method described in Section 4 (see Eqs. (20) and (21)) computes the target pivot displacement $\bar{x}_p(t)$ with a feedback gain matrix **G**. Table 2 shows the control parameters of the LSCMD, which include the design parameters and the determined discrete-time control gain matrix **G** .The chosen control delay time t_d of the LSCMD is 0.1 s, which was obtained from the identified transfer function described in Section 5.2. In the design of the weight matrix **Q**, both of the potential energy and kinetic energy can be chosen. However, the objective of the LSCMD is to mitigate the peak stroke and story drift which are related to the potential energy. Therefore, only the potential energy is considered in the weight matrix **Q**. The LQR control using full state feedback may be a challenge for a structural system with a large number of DOFs, because a large amount of sensors is required for computing the control force. For this reason, a LQR control with direct output-feedback which requires only some chosen state variables of the controlled system is more suitable. In this study, the LSCMD stroke and its velocity are selected to be the feedback measurements of the controlled system. In the case, the sensor placement matrix for the LSCMD is

$$\mathbf{D} = \begin{bmatrix} 0 & 1 & 0 & 0 \\ 0 & 0 & 0 & 1 \end{bmatrix} \quad (26)$$

6.3 Selection of ground excitations

The following two types of ground excitation were considered in the experiment: (1) white-noise earthquake (peak ground acceleration (PGA)=120 gal); (2) 1999

Table 2 Control parameters of LSCMD

Parameter		Value
Weighting factors used in LQR controller design	**Q**	$\begin{bmatrix} \mathbf{K} & \mathbf{0} \\ \mathbf{0} & \mathbf{0} \end{bmatrix}$
	R	10^{-4}
Control delay time, t_d (s)		0.1
Control gain matrix, **G** [N/m, N·s/m]		[8.6319, -9.8663]

Chi-Chi (station TCU076) earthquake (PGA=120 gal). The allowable mass damper stroke of the prototype LSCMD is limited about 100 mm, so the PGA of the ground excitations is considered based on the stroke limitation. The experimental results of the passive TMD under the white-noise and Chi-Chi earthquakes are used to verify the optimal parameters of the passive TMD which are derived for white-noise earthquakes (Warburton 1982). The comparisons of experimental results under the two earthquakes between the passive TMD and the LSCMD are used to verify the control performance of the LSCMD. Figs. 8 and 9 depict the waveforms and frequency spectra of the two earthquakes which are the measured ground accelerations in the shaking-table test, respectively Fig. 8 shows that the ground motion of the white-noise earthquake has high intensity in the frequency range of 1-30 Hz. Fig. 9 shows that the ground motion of the Chi-Chi earthquake has high intensity in the frequency range of 1-10 Hz.
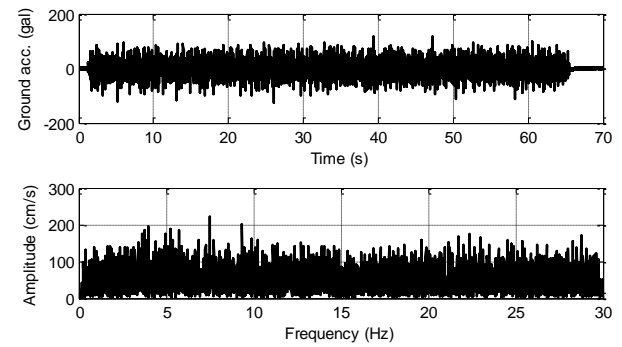

Fig. 8 Time histories and frequency spectra of white-noise earthquake (PGA=120 gal)
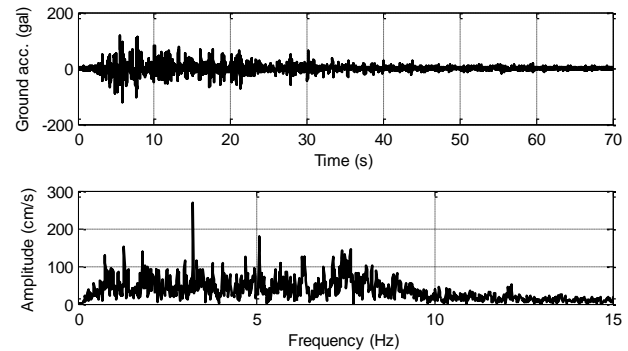

Fig. 9 Time histories and frequency spectra of 1999 Chi-Chi (TCU076) earthquake (PGA=120 gal)

7. Test results and discussion

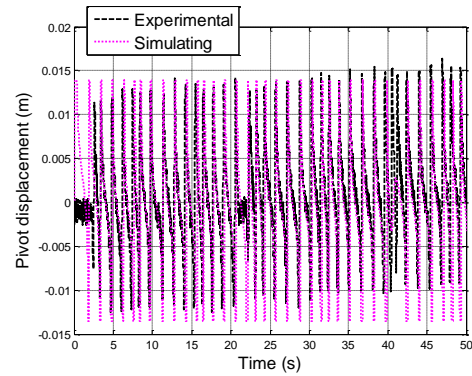### 7.1 Comparison of experimental and simulating results

In this section, a comparison of the experimental and simulating results is conducted to verify the proposed LSCMD theoretical model and numerical analysis method. The simulating results are obtained using the numerical analysis method described in Section 2 and the parameters listed in Tables 1 and 2. The sampling rate used in the numerical analysis is 200 Hz, which is the same as that of the data acquisition system in the shaking-table test.

Figs. 10 and 11 compare the simulating results and experimental results for the white-noise and Chi-Chi earthquakes, respectively. The figures show the time histories of the story drift $x_s(t)$, mass damper stroke $x_{ds}(t)$, pivot displacement $x_p(t)$, and the hysteresis loop of the LSCMD, which represents the relationship between $x_{ds}(t)$ and the semi-active control force $u_c(t)$. The semi-active control force $u_c(t)$ was computed from the measured pivot displacement and mass damper stroke (see Eqs. (11) and (12)).

Figs. 10 and 11 show that: (1) in subplots (a) and (b), the experimental results of the LSCMD system can be simulated by the theoretical model; (2) in subplot (c), the pivot displacement can be manipulated as expected by the control law during the whole control process; (3) in subplot (d), the compatible results prove that the semi-active control force $u_c(t)$ and variable stiffness increment $\Delta k_d(t)$ are regulated by controlling the pivot displacement $x_p(t)$, even if there is a minor deviation between the experimental and simulating hysteresis loops of the LSCMD. Additionally, the equivalent damping does not cause a larger deviation in the system's responses, as shown in subplots (a) and (b). The pivot is driven by the servo motor, the major drawback is the servo motor produced a large amounts of electrical noise which are high frequency signals and interfere with sensor signals. The high frequency and small amplitude oscillation shown in the experimental results of a long-period structure may be caused by the electrical noise.
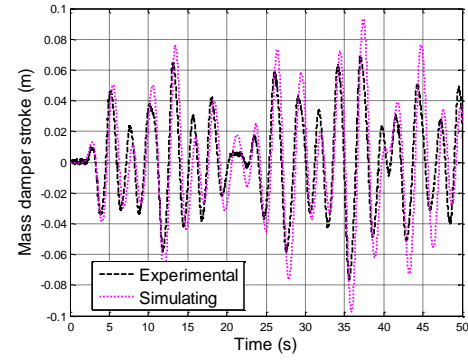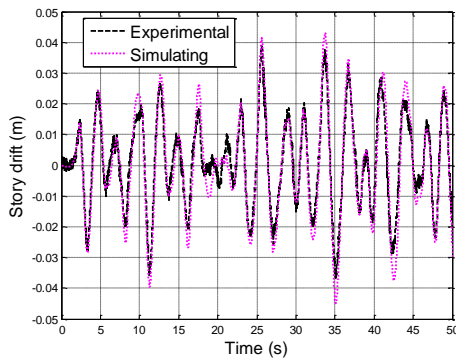

(b) Mass damper stroke
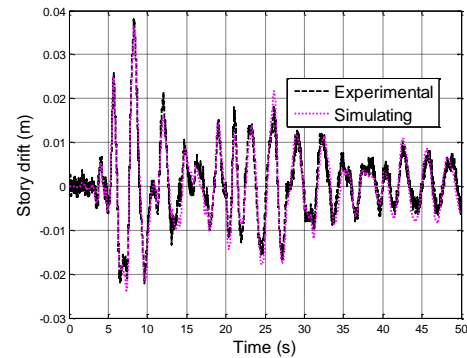

(c) Pivot displacement
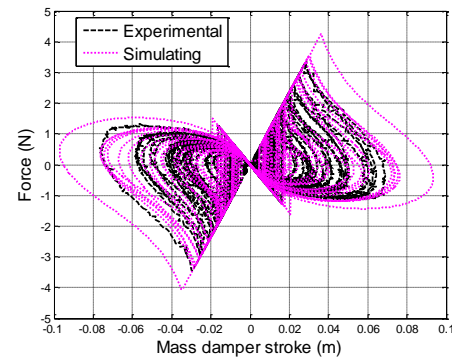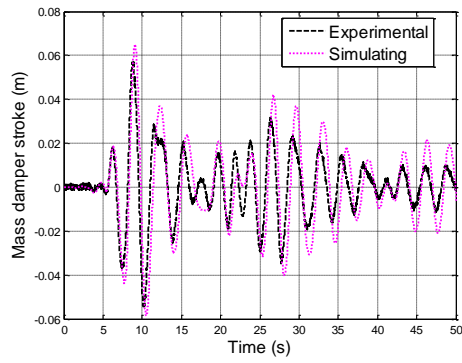

(d) Hysteresis loop

Fig. 10 Continued

(a) Story drift

Fig. 10 Comparison of simulating and experimental results for LSCMD (white-noise earthquake, PGA=120 gal)
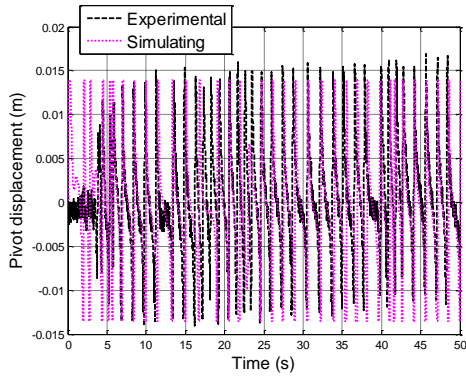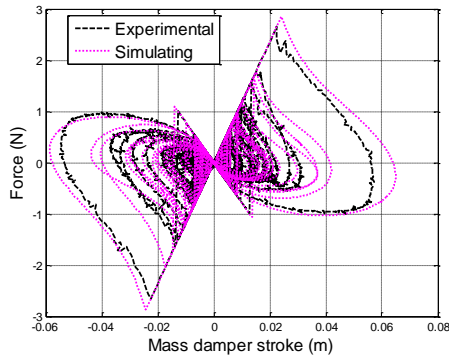

(a) Story drift

Fig. 11 Comparison of simulating and experimental results for LSCMD (Chi-Chi (TCU076) earthquake, PGA=120 gal)
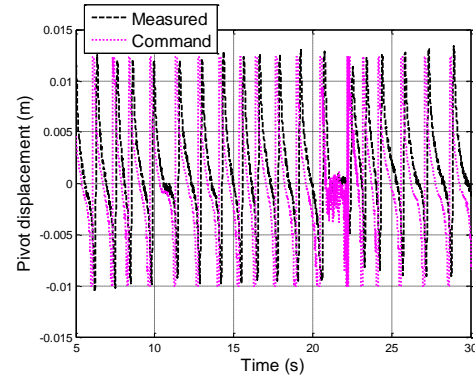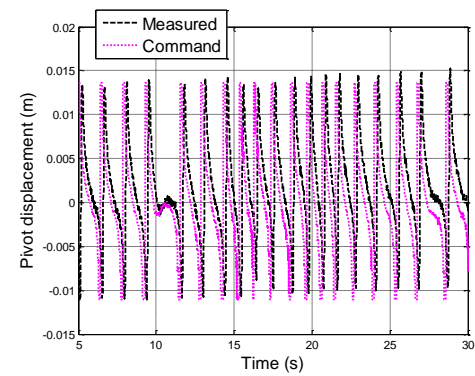
(b) Mass damper stroke

(a) White-noise earthquake

(c) Pivot displacement

(b) Chi-Chi (TCU076) earthquake

Fig. 12 Comparison of command and measured pivot displacement.

(d) Hysteresis loop

Fig. 11 Continued

following section, the control performance of the LSCMD will be evaluated.

7.2 Evaluation of LSCMD control performance

In order to evaluate the control performance of the LSCMD, the experimental results of the prototype LSCMD are compared with those of a passive TMD system. The parameters of the passive TMD system, which are the same as those of the LSCMD (see Tables 1 and 2), were tested using a shaking table with the same earthquakes. Figs. 13 and 14 show the time history comparisons of the LSCMD and passive TMD systems under the two earthquakes, respectively. The story drift $x_s(t)$ is shown in subplot (a) and the mass damper stroke is shown in subplot (b). As indicated in Figs. 13 and 14, the LSCMD and passive TMD systems have almost the same peak story drift. However, the peak strokes of the LSCMD (77 and 57 mm), shown in Figs. 13(b) and 14(b), are suppressed than those of the passive TMD (90 and 66 mm) by about 14 %. This demonstrates that the mass damper stroke of the LSCMD was successfully alleviated by adjusting the LSCMD stiffness with the active control law. However, the control performance of the LSCMD is not significant because of the large damping at its passive mode. The same conclusions can be found in a detailed numerical investigations (Chu *et al.* 2017).

Because the limitation of the LSCMD stoke, the LSCMD with large PGA earthquakes can not be tested. To

Fig. 12 compares the commanded and measured pivot displacements for the same tests in Figs. 10 and 11. Even there is a spike in the vicinity of 1.3 Hz of the identified normalized amplitude as shown in Fig. 6(a), Fig. 12 demonstrates that the measured pivot displacement is able to closely follow the control command determined by the control law. Although the minor oscillation can be observed in the pivot displacement that may be amplified due to the noise, the upper and lower bounds of the pivot displacement can be regulated well since the dominated frequencies of the LSCMD stroke and its velocity are within the vicinities of 0.3 Hz and 0.4 Hz as tabulated in Table 1, respectively. This proves that the driving and control systems have good performance for the current long-period (0.37 Hz) specimen, further lead-lag compensator can be adopted to improve the undesirable frequency responses when a short-period main structure specimen will be used. In the

Table 3 Comparison of peak and RMS responses for different TMD systems

Earthquake	System	Responses*			
		Story drift x_s (mm)		TMD stroke x_{ds} (mm)	
		Peak	RMS	Peak	RMS
White Noise (PGA = 300gal)	Uncontrolled	247 (1.00)	91 (1.00)	--	--
	Passive TMD	101 (0.41)	40 (0.44)	249 (1.00)	99 (1.00)
	LSCMD	108 (0.44)	41 (0.45)	231 (0.93)	86 (0.87)
Chi-Chi TCU076 (PGA = 300gal)	Uncontrolled	106 (1.00)	34 (1.00)	--	--
	Passive TMD	87 (0.82)	19 (0.56)	178 (1.00)	50 (1.00)
	LSCMD	89 (0.84)	19 (0.56)	156 (0.88)	42 (0.84)
El Centro (PGA = 300gal)	Uncontrolled	370 (1.00)	189 (1.00)	--	--
	Passive TMD	224 (0.61)	63 (0.33)	560 (1.00)	187 (1.00)
	LSCMD	237 (0.64)	72 (0.38)	473 (0.84)	167 (0.89)
Northridge (PGA = 300gal)	Uncontrolled	341 (1.00)	137 (1.00)	--	--
	Passive TMD	230 (0.67)	57 (0.42)	573 (1.00)	143 (1.00)
	LSCMD	231 (0.68)	59 (0.43)	491 (0.86)	123 (0.86)

*A value in parenthesis represents the response ratio of a specific system over the uncontrolled or passive response

(a) Story drift

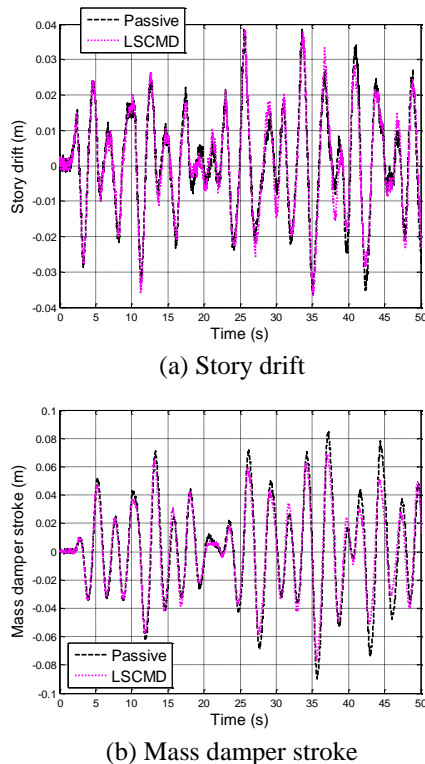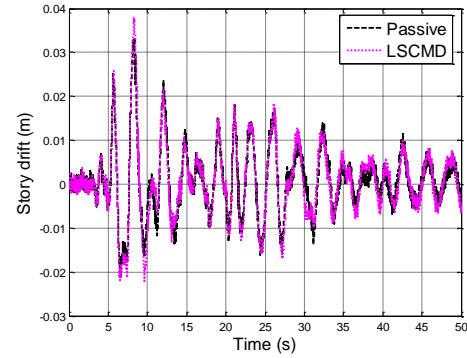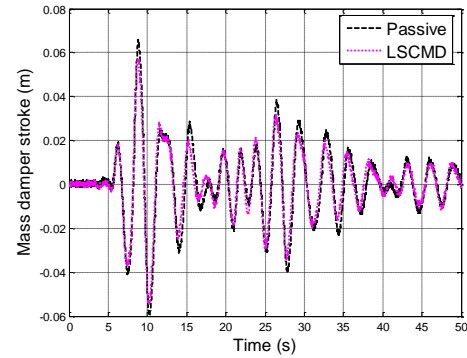

(b) Mass damper stroke

Fig. 13 Comparison of LSCMD and passive TMD (white-noise earthquake, PGA=120 gal)

(a) Story drift

(b) Mass damper stroke

Fig. 14 Comparison of LSCMD and passive TMD (Chi-Chi (TCU076) earthquake, PGA=120 gal)

verify the control performance of the prototype LSCMD, the responses of the LSCMD system under four types of earthquakes with PGA=300 gal are simulated. The four types of recorded ground excitations includes (1) White Noise and 1999 Chi-Chi earthquake which are recorded in the shaking table tests; (2) 1940 El Centro earthquake and 1994 Northridge earthquake which are the famous far-field and near-fault earthquakes. Table 3 compares the peak and root-mean-square (RMS) response values of the three systems: uncontrolled, the passive TMD and the LSCMD. As shown in Table 3, a value in parenthesis represents the peak and RMS response ratio of a specific system over the uncontrolled or passive response. The table indicates that (1) both passive TMD and LSCMD systems have almost the same reduction on peak and RMS story drift by about 16%-59% in the four earthquakes; (2) when compared to the passive TMD system, the LSCMD is able to reduce the peak and RMS TMD stroke by about 7%-16%. This shows that even with the inherent damping ratio 0.17, a better performance on TMD stroke reduction still can be achieved by the LSCMD.

8. Conclusions

In order to verify the feasibility of a SATMD under earthquake excitations, a variable-stiffness tuned mass damper that utilized a leverage mechanism was fabricated and tested by a shaking-table test in this study. The

proposed LSCMD has a lever arm with a movable pivot. The ratio of the lever arm can be varied by adjusting the pivot displacement. As a result, the equivalent stiffness of the LSCMD can be controlled in real time, making the LSCMD more adaptive than a passive TMD. Before performing the shaking-table test, the system parameters and the transfer function of the LSCMD were identified. An active control law (the optimal control with direct output-feedback and consideration of the control delay time) was implemented to compute the target semi-active force, which is used to determine the target pivot displacement for the LSCMD. The comparisons of experimental and theoretical results of the LSCMD system demonstrate that the shaking-table results of the LSCMD system can be simulated by the theoretical model and the time histories of both the story drift and mass damper stroke are predicted well. The comparisons of the LSCMD and passive TMD system demonstrate that the LSCMD led to less demand on the damper stroke than the passive TMD did.

Acknowledgements

References

Chey, M.H., Rodgers, G.W., Chase, J.G. and Mander, J.B. (2010), "Using upper storeys as semi-active tuned mass damper building systems - A case study analysis", *Bull. NZ. Soc. Earthq. Eng.*, **43**(2), 126-133.

Chu, S.Y., Lin, C.C., Chung, L.L., Chang, C.C. and Lu, K.H. (2008), "Optimal performance of discrete-time direct output-feedback structural control with delayed control forces", *Struct. Control Hlth.*, **15**(1), 20-42.

Chu, S.Y., Soong, T.T. and Reinhorn, A.M. (2005), *Active, Hybrid, and Semi-active Structural Control: a Design and Implementation Handbook*, Wiley, New York, NY, USA.

Chu, S.Y., Soong, T.T., Lin, C.C. and Chen, Y.Z. (2002), "Time-delay effect and compensation on direct output feedback controlled mass damper systems", *Earthq. Eng. Struct. Dyn.*, **31**(1), 121-137.

Chu, S.Y., Yeh, S.W., Lu, L.Y. and Peng, C.H. (2017), "A leverage-type stiffness controllable mass damper for vibration mitigation of structures", *Struct. Control Hlth.*, **24**(4), e1896.

Chung, L.L., Lai, Y.A., Walter Yang, C.S., Lien, K.H. and Wu, L.Y. (2013b), "Semi-active tuned mass dampers with phase control", *J. Sound Vib.*, **332**(15), 3610-3625.

Chung, L.L., Wu, L.Y., Yang, C.S.W., Lien, K.H., Lin, M.C. and Huang H.H. (2013a), "Optimal design formulas for viscous tuned mass dampers in wind-excited structures", *Struct. Control Hlth.*, **20**(3), 320-336.

Deshmukh, S.N. and Chandiramani, N.K. (2014), "LQR control of wind excited benchmark building using variable stiffness tuned mass damper", *Shock Vib.*, **2014**.

Gonzalez-Buelga, A., Clare, L.R., Cammarano, A., Neild, S.A., Burrow, S.G. and Inman, D.J. (2014), "An optimised tuned mass damper/harvester device", *Struct. Control Hlth. Monit.*, **21**(8), 1154-1169.

Ito, M., Yoshida, S., Fujitani, H. and Sato, Y. (2015), "Earthquake response reduction of mid-story isolated system due to semi-active control using magnetorheological rotary inertia mass damper", *Active and Passive Smart Structures and Integrated Systems*, San Diego, CA, United states, April.

Kang, J., Kim, H.S. and Lee, D.G. (2011), "Mitigation of wind response of a tall building using semi-active tuned mass dampers", *Struct. Des. Tall Spec. Build.*, **20**(5), 552-565.

Korkmaz, S. (2011), "A review of active structural control: challenges for engineering informatics", *Comput. Struct.*, **89**(23-24), 2113-2132.

Li, L., Geng, C., Tian Y. and Yu, Q. (2012), "Vibration control effect analysis on tuned mass damper system used in urban transportation", *Adv. Mater. Res*, **468-471**, 1294-1299.

Lin, C.C., Lu, L.Y., Lin, G.L. and Yang, T.W. (2010), "Vibration control of seismic structures using semi-active friction multiple tuned mass dampers", *Eng. Struct.*, **32**(10), 3404-3417.

Lin, G.L., Lin, C.C., Chen, B.C. and Soong, T.T. (2015), "Vibration control performance of tuned mass dampers with resettable variable stiffness", *Eng. Struct.*, **83**, 187-197.

Lin, G.L., Lin, C.C., Lu, L.Y. and Ho, Y.B. (2012), "Experimental verification of seismic vibration control using a semi-active friction tuned mass damper", *Earthq. Eng. Struct. Dyn.*, **41**(4), 813-830.

Lin, P.Y., Lin, T.K. and Hwang, J.S. (2013), "A semi-active mass damping system for low- and mid-rise buildings", *Earthq. Struct.*, **4**(1), 63-84.

Liu, Y., Zuo, L. and Tang, X. (2013), "Regenerative vibration control of tall buildings using Model Predictive Control", *Dynamic Systems and Control Conference*, Palo Alto, CA, United states, October.

Lu, L.Y., Chu, S.Y., Yeh, S.W. and Chung, L.L. (2012), "Seismic test of least-input-energy control with ground velocity feedback for variable-stiffness isolation systems", *J. Sound Vib.*, **331**(4), 767-784.

Majcher, K. (2014), "The influence of changing stiffness characteristic of a semi-Active tuned mass damper onto the effectiveness of vibration reduction in a plate-column structure", *23rd Russian-Polish-Slovak Seminar on Theoretical Foundation of Civil Engineering*, Wroclaw, Szklarska Poreba, Poland, August.

Marano, G.C. and Greco, R. (2011), "Optimization criteria for tuned mass dampers for structural vibration control under stochastic excitation", *J. Vib. Control*, **17**(5), 679-688.

Moghaddas, M., Esmailzadeh, E., Sedaghati, R. and Khosravi, P. (2011), "Vibration control of Timoshenko beam traversed by moving vehicle using optimized tuned mass damper", *J. Vib. Control*, **18**(6), 757-773.

Nagarajaiah, S. and Sonmez, E. (2007), "Structures with semiactive variable stiffness single/multiple tuned mass dampers", *J. Struct. Eng.*, **133**(1) 67-77.

Nagarajaiah, S. and Varadarajan, N. (2005), "Short time Fourier transform algorithm for wind response control of buildings with variable stiffness TMD", *Eng. Struct.*, **27**(3), 431-441.

Pasala, D.T.R. and Nagarajaiah, S. (2014), "Adaptive-length pendulum smart tuned mass damper using shape-memory-alloy wire for tuning period in real time", *Smart Struct. Syst.*, **13**(2), 203-217.

Rakicevic, Z.T., Bogdanovic, A., Jurukovski, D. and Nawrotzki, P. (2012), "Effectiveness of tune mass damper in the reduction of the seismic response of the structure", *Bull. Earthq. Eng.*, **10**(3), 1049-1073.

Soleymani, M. and Khodadadi, M. (2014), "Adaptive fuzzy controller for active tuned mass damper of a benchmark tall building subjected to seismic and wind loads", *Struct. Des. Tall Spec. Build.*, **23**(10), 781-800.

Wang, J.F., Lin, C.C. and Chen, B.L. (2003), "Vibration suppression for high-speed railway bridges using tuned mass dampers", *Int. J. Solid. Struct.*, **40**(2), 465-491.

Warburton, G.B. (1982), "Optimum absorber parameters for various combinations of response and excitation parameters", *Earthq. Eng. Struct. Dyn.*, **10**(3), 381-401.

KT